MAGNETOHYDRODYNAMICS Vol. 48 (2012), No. 2, pp. 313–320

SIMULATION OF THE INFLUENCE OF ELECTROMAGNETIC FIELDS ON THE DRAINAGE IN WET METAL FOAM

S. Heitkam[1,2], *S. Schwarz*[1], *J. Fröhlich*[1]

[1] *Institut für Strömungsmechanik, TU Dresden, 01062 Dresden, Germany*
[2] *Université Paris Sud, Laboratoire de Physique des Solides (UMR 8502), 91405 Orsay, France*

The paper reports on numerical simulations of stationary drainage through agglomerated bubbles under the influence of a horizontal magnetic field. A linear relation between the pressure drop and the drainage flow is found, while the influence of the magnetic field on the pressure drop is quadratic. At low pressure drops the bubbles agglomerate in tightly packed clusters. Crystalline arrangement has been observed between 10 and 30 percent. Higher drainage rate and higher magnetic fields both make the bubbles oscillate around their position in the packing and thus decrease the gas fraction.

Introduction. The paper is motivated by the creation of metal foam via injection of gas bubbles at the bottom of a container filled with a liquid metal [1]. In this process, excessive drainage can result in bubble rupture and inhomogeneity of the final material. Hence, the control of drainage in liquid metal foam is desired. It is well known that the motion of conducting liquids can be damped by a transverse magnetic fields [2–6], but the influence of such a field on the drainage in metal foam has not yet been investigated. Since liquid metal is opaque, measurements in liquid foam are very challenging [7]. Quasi-steady bubble distributions and slow drainage processes can be investigated by tomography [8, 9]. But information about the flow structure in the plateau borders including induced electrical currents in the magnetic field are not available so far. Numerical simulations are exempt of this problem and allow to investigate bubble motion, velocity and pressure fields inside the foam in great detail as well as effects of a magnetic field being applied. This is the focus of the present paper.

1. Simulation method. The multiphase code PRIME [10–12] is based on a staggered grid arrangement in the Cartesian coordinates and utilizes a second-order finite volume method. The incompressible Navier–Stokes equations including the Lorentz force

$$\frac{\partial \mathbf{u}}{\partial t} + (\mathbf{u}\mathrm{div})\mathbf{u} = \frac{1}{\rho_\mathrm{f}} \operatorname{grad} p + \nu \operatorname{grad} \mathrm{div}\mathbf{u} + \frac{1}{\rho_\mathrm{f}} \mathbf{j} \times \mathbf{B} + \mathbf{f}, \tag{1}$$

$$\mathrm{div}\mathbf{u} = 0, \tag{2}$$

are solved using a Runge–Kutta three-step method with implicit treatment of the viscous terms. There, $\mathbf{u}$ is the fluid velocity, ρ_f is the fluid density, p denotes pressure, ν is the fluid viscosity and $\mathbf{B}$ is the magnetic field. The Ohm's law for low magnetic Reynolds numbers allows to express the electric current $\mathbf{j}$ as

$$\mathbf{j} = \alpha\, \sigma_\mathrm{el}(\mathbf{u} \times \mathbf{B} - \operatorname{grad} \phi). \tag{3}$$

Here, $\alpha \in [0, 1]$ represents a phase indicator and σ_el is the electric conductivity of the liquid. The former is obtained from a second-order accurate approach

for the calculation of the cut cell volumes using a level set representation of the phase interface [11]. The conductivity of the immersed bubbles is set to zero. Charge conservation $\mathrm{div}\mathbf{j} = 0$ is maintained by solving a Poisson equation for the electric potential ϕ on the Eulerian grid, accounting for jumps in σ_{el} by an iterative procedure.

The treatment of bubbles is based on an Euler–Lagrange approach, in which the shape of the particle is resolved with its surface represented by Lagrangian marker points. Coupling between the continuous liquid metal phase and the embedded bodies is realized via an Immersed Boundary Method (IBM) [10, 13], which imposes no-slip boundary condition at the bubbles surface by adding additional volume forces $\mathbf{f}$ in Eq. (1). The counterparts of these forces act on the corresponding bubble, which is treated as a light rigid sphere by solving its linear and angular momentum equation

$$m_{\mathrm{b}} \frac{\mathrm{d}\mathbf{u}_{\mathrm{b}}}{\mathrm{d}t} = \rho_{\mathrm{f}} \oint_{\Gamma} \mathbf{f} \mathrm{d}s + V_{\mathrm{b}}(\rho_{\mathrm{b}} - \rho_{\mathrm{f}})\mathbf{g} - \mathbf{F}_{\mathrm{int}} \tag{4}$$

$$\frac{m_{\mathrm{b}} D^2}{4} \frac{\mathrm{d}\boldsymbol{\omega}_{\mathrm{b}}}{\mathrm{d}t} = \rho_{\mathrm{f}} \oint_{\Gamma} [\mathbf{r} \times \mathbf{f}] \mathrm{d}s - \mathbf{M}_{\mathrm{int}}, \tag{5}$$

where $\mathbf{u}_{\mathrm{b}} = \mathrm{d}\mathbf{x}_{\mathrm{b}}/\mathrm{d}t$ is the velocity of the bubble center and $\boldsymbol{\omega}_{\mathrm{b}}$ is the angular velocity of the bubble. $\mathbf{F}_{\mathrm{int}}$ and $\mathbf{M}_{\mathrm{int}}$ represent the integrated action on the liquid inside the bubble. In case of bubble contact, a conservative repulsive force $\mathbf{F}_{\mathrm{coll}}$ is added in the linear momentum equation (4). It acts in the centers $\mathbf{x}_i$ and $\mathbf{x}_k$ of the bubbles i and k, respectively, and is normal to the contact tangential plane

$$\mathbf{F}_{\mathrm{coll},k} = -\mathbf{F}_{\mathrm{coll},i} = \min[0, 2\pi(|\mathbf{x}_i - \mathbf{x}_k| - D - 2r_s)] \frac{(\mathbf{x}_i - \mathbf{x}_k)}{|\mathbf{x}_i - \mathbf{x}_k|}. \tag{6}$$

The additional safety clearance $r_s = 0.05D$ is used here to prevent bubbles from overlapping.

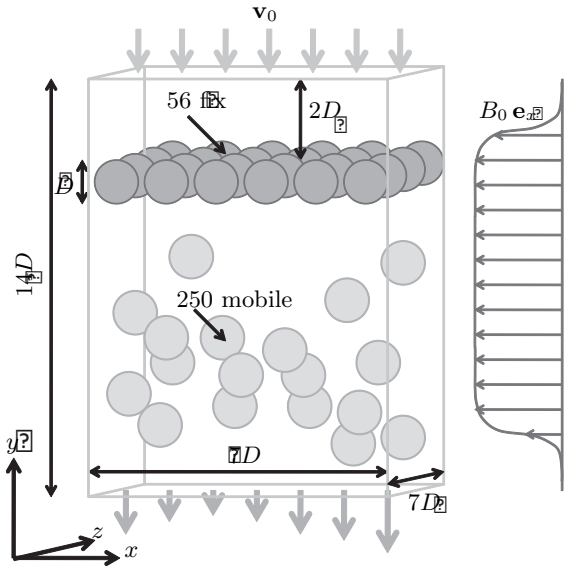

Fig. 1. Geometrical setup of the drainage simulation.

Table 1. Physical and numerical parameters of the setup.

quantity	symbol	value	unit
bubble diameter	D	2×10^{-3}	m
electrical conductivity	σ_{el}	5×10^{5}	$S\ m^{-1}$
fluid viscosity	ν	5×10^{-7}	$m^2\ s^{-1}$
gravitational acceleration	g	9.81	$m\ s^{-2}$
fluid density	ρ_{f}	2400	$kg\ m^{-3}$
drainage velocity	v_0	10^{-3} *to* 2×10^{-2}	$m\ s^{-1}$
gas density	ρ_g	1.2	$kg\ m^{-3}$
magnetic field	B	10^{-3} *to* 10^{-1}	T
surface tension	σ	1	$N\ m^{-1}$
domain size	$L_x \times L_y \times L_z$	$7D \times 14D \times 7D$	-
domain resolution	$N_x \times N_y \times N_z$	$256 \times 512 \times 256$	-
number of surface markers	N_L	4208	–

2. Setup. In order to investigate steady behaviour of metal foam, a setup with a constant drainage flow rate was designed similar to [14]. Fig. 1 shows the arrangement with the constant drainage velocity v_0 directed downward through the computational domain. Boundary conditions in horizontal directions are periodic. At the top, 56 immobile bubbles are arranged in regular closest planar packing. Below, 250 mobile bubbles are randomly positioned and successively released one after another starting with the highest ones, so that they rise and agglomerate below the fixed bubbles. The present investigations were carried out when all bubbles were released and a stationary state for the pressure drop had been reached.

A constant horizontal magnetic field is imposed on the domain. Near the top and bottom of the domain the magnetic field smoothly tends toward zero in order to get smooth in- and outflow conditions. At the boundaries, the normal derivatives of the electric potential ϕ are set to zero. The physical parameters of the setup are given in Table 1. They are chosen to represent liquid aluminum [15]. Table 1 also provides information on the spatial discretization of the computational domain and the number of surface markers per bubble employed. The time step used in the simulations was $\Delta t = 1 \times 10^{-4}$ s.

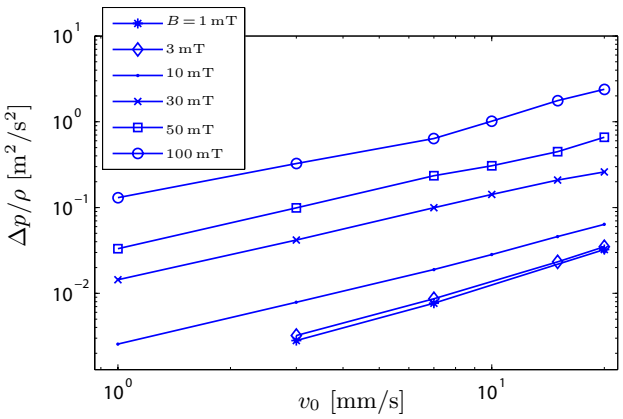

Fig. 2. Pressure drop versus the drainage velocity.

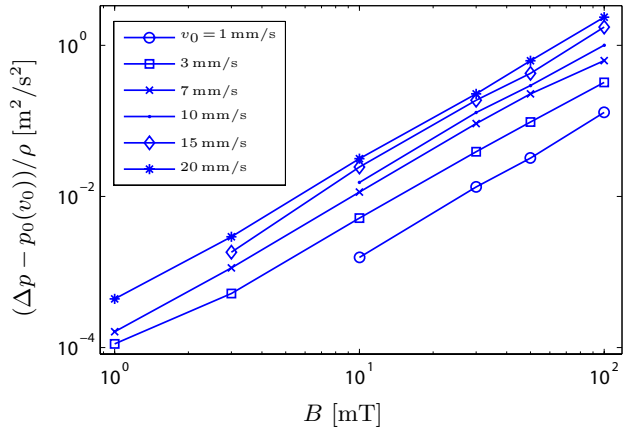

Fig. 3. Increment of the pressure drop versus the magnetic field strength.

3. Results. To determine the total pressure drop Δp that is caused by the agglomerated bubbles, the averaged pressure difference between the top and bottom of the domain is calculated and reported in Fig. 2. The slope in the double-logarithmic plot corresponds to a linear relationship between pressure loss and drainage velocity. Two effects add to the pressure drop. On the one hand, there is a drainage resistance Δp_0 of the foam without the magnetic field that is shown in Fig. 2 by the data with a negligibly small magnetic field B of 1 and 3 mT. On the other hand, the magnetic field causes a pressure drop that is also proportional to the drainage velocity. To extract the second effect, the natural drainage resistance Δp_0 (obtained from the case $B = 1$ mT) is subtracted from the total pressure drop. Fig. 3 shows the resulting pressure drop versus the strength of the magnetic field. The slope in this graph is almost constant and corresponds to a quadratic relationship so that for the total pressure loss the following ansatz is made:

$$\frac{\Delta p}{\rho_\mathrm{f}} = v_0(C_1 + C_2 B^2). \tag{7}$$

The values for C_1 and C_2 have been determined by least-squares-fitting, yielding $C_1 = 1.2$ m/s and $C_2 = 104$ m/(sT^2). The case without the magnetic field, Δp_0, is characterized by C_1 only so that $\Delta p_0 = \rho_\mathrm{f} v_0 C_1$ can also be related to the Darcy's law [16]

$$v_0 = \frac{k_\mathrm{f}}{gH}\frac{\Delta p_0}{\rho_\mathrm{f}}, \tag{8}$$

where $H \approx 6D = 0.012$ m is the thickness of the packing. Comparing Eq. (7) with Eq. (8) for $\Delta p = \Delta p_0$ yields $k_\mathrm{f} = gH/C_1$. For the simulation conducted, this results in a value of $k_\mathrm{f} \approx 0.1$ m/s. Independently, k_f was determined using a relation for randomly packed particles [16] and a viscosity correction according to [17] giving $k_\mathrm{f} = 0.09$ m/s. The value obtained from the simulation is close to this empirical one, showing that indeed the simulation is realistic.

The agglomerated bubbles are now characterized in terms of their mobility and density. The mobility is quantified by the standard deviation of the velocity of the bubbles when they oscillate around their mean position. This quantity reported in Fig. 4 is obtained by averaging in time and over all mobile bubbles. Each symbol in Figs. 4, 5 and 6 corresponds to one simulation in Fig. 2. In Fig. 4, an increase of mobility with the increasing pressure drop is clearly visible. Furthermore, the magnitude of the fluctuations in both horizontal directions, x and z, is very similar.

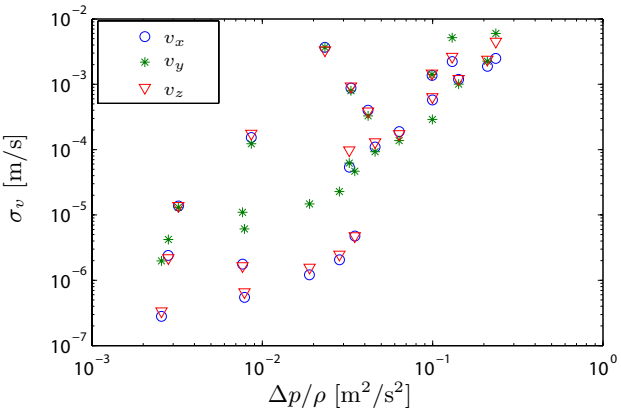

Fig. 4. Standard deviation of the three velocity components versus the pressure drop.

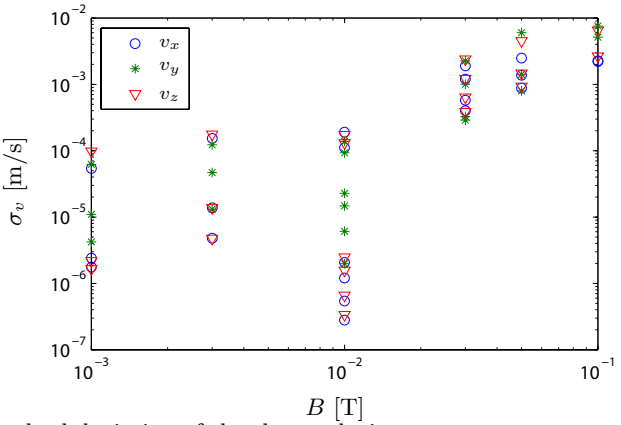

Fig. 5. Standard deviation of the three velocity components versus the magnetic field strength.

This isotropy is remarkable since the magnetic field is oriented in the x-direction. It should hence damp fluctuations in the z-direction more than in the x-direction as observed for wakes [12]. In most cases, the mobility in the vertical direction (y) is higher, which is expected as the fluid force dominantly acts in this direction. An increase of the mobility with the increasing strength of the magnetic field has also been found as reported in Fig. 5. This fact is against the general observation that magnetic fields damp the movement of conducting fluids [2, 3, 5] and might arise from the fact that the magnetic field increases the pressure drop and thus the mobility according to Fig. 4.

By a separate investigation, it was found that the packing density of the mobile bubbles was practically constant over the height so that subsequently the gas fraction Φ_{gas} was determined by averaging the position of the lowest mobile bubbles to get the volume occupied by the mobile bubbles. Fig. 6 shows that Φ_{gas} is almost independent of the pressure drop over a wide range of local pressure drops ($\Phi_{\text{gas}} \approx 0.62$ for $\Delta p/\rho \approx 10^{-2}\,\text{m}^2\text{s}^{-2}$). For the medium pressure drop, the gas fraction decreases because of the increasing bubble motion. Against this general trend, three simulations lead to a higher gas fraction (marked symbols in Fig. 6). By analyzing local neighbourhood conditions it has been found that this reflects an arrangement in the crystalline structure to a larger extent than in the

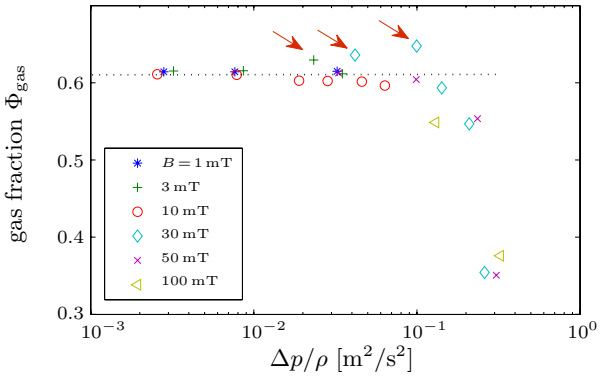

Fig. 6. Volume fraction of mobile bubbles versus the pressure drop. The dotted line indicates the gas fraction at lowest pressure loss. Arrows point to cases with particularly high crystalline order.

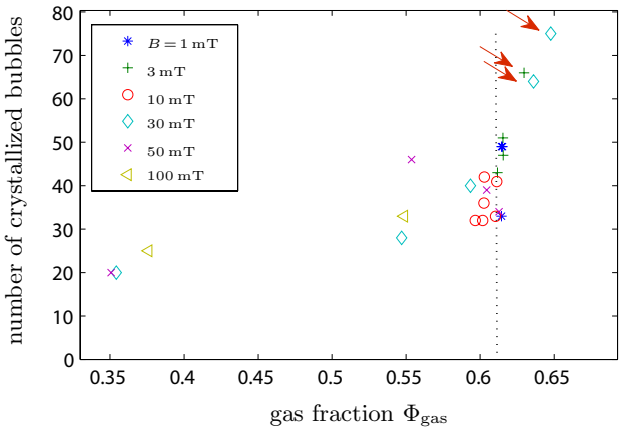

Fig. 7. Number of bubbles in crystalline arrangement versus the volume fraction of mobile bubbles. The dotted line indicates the gas fraction at lowest pressure loss. Arrows point to cases with particularly high volume fraction.

other cases, as presented in Fig. 7. No systematic dependency of this feature on parameters of the simulation was found. Higher pressure drop creates higher forces on the bubbles and makes the bubbles float, which, in turn, strongly decreases the gas fraction.

4. Conclusions. The paper presents numerical simulations of wet foams of liquid metals. Without the magnetic field, the pressure drop resulting from imposed drainage through the agglomerated bubbles depends linearly on the drainage velocity. The results are in good agreement with the Darcy's law, which validates the approach. A relatively low transverse magnetic field can increase the pressure drop significantly, which furthermore is shown to be proportional to the square of the field strength. The magnetic forces and the fluid forces on the bubbles increase the mobility of the bubbles. This can lead to increased crystalline ordering. Above a critical pressure drop the bubbles start to float. Similar experimental results are not available at present due to obvious difficulties of experiments in liquid metal foams. The present study was focused on macroscopic quantities like pressure drop and gas fraction. The future work will be concerned with analyzing the flow field

and the electric current, as well as the crystalline order according to the approach in [18].

Acknowledgments. We greatly acknowledge the considerable effort of Tobias Kempe developing the code PRIME. This work was funded by the DFG via the collaborative research center SFB 609.

REFERENCES

[1] M.F. Ashby. *Metal foams: a design guide.* (Butterworth-Heinemann, 2000).

[2] T. Weier *et al.* On stability of the MHD flow around a cylinder in an aligned magnetic field. *Magnetohydrodynamics*, vol. 33 (1997), no. 1, pp. 11–18.

[3] G. Mutschke, V. Shatrov, and G. Gerbeth. Cylinder wake control by magnetic fields in liquid metal flows. *Experimental Thermal and Fluid Science*, vol. 16 (1998), no. 1-2, pp. 92–99.

[4] P.M. Blosseville, S. Aleksandrova, and S. Molokov. Buoyancy-driven MHD flow in electrically insulated rectangular ducts. *Magnetohydrodynamics*, vol. 43 (2007), no. 3, pp. 315–321.

[5] S. Schwarz and J. Fröhlich. Numerical simulation of MHD flow around fixed and freely ascending spheres and ellipsoids. In: *The 8th PAMIR International Conference on Fundamental and Applied MHD*, (2011).

[6] T. Boeck, D. Krasnov, and E. Zienicke. Numerical study of turbulent magnetohydrodynamic channel flow. *Journal of Fluid Mechanics*, vol. 572 (2007), pp. 179–188.

[7] O. Brunke and S. Odenbach. In situ observation and numerical calculations of the evolution of metallic foams. *Journal of Physics-Condensed Matter*, vol. 18 (2006), no. 28, pp. 6493–6506.

[8] J. Banhart, H. Stanzick, L. Helfen, and T. Baumbach. Metal foam evolution studied by synchrotron radioscopy. *Applied Physics Letters*, vol. 78 (2001), no. 8, pp. 1152–1154.

[9] H. Stanzick, J. Klenke, S. Danilkin, and J. Banhart. Material flow in metal foams studied by neutron radioscopy. *Applied Physics, Materials Science & Processing*, vol. 74 (2002), pp. S1118–S1120.

[10] T. Kempe and J. Fröhlich. An improved immersed boundary method with direct forcing for the simulation of particle laden flows. *Journal of Computational Physics*, vol. 231 (2012), pp. 3663–3684.

[11] T. Kempe, J. Schwarz, and J. Fröhlich. Modelling of spheroidal particles in viscous flow. In *Academy Colloquium Immersed Boundary Methods: Current Status and Future Research Directions.* (Amsterdam, the Netherlands, 2009).

[12] S. Schwarz and J. Fröhlich. DNS of single bubble motion in liquid metal and the influence of a magnetic field. In: *The 7th International Symposium on Turbulence and Shear Flow Phenomena* (Ottawa, Kanada, 2011).

[13] M. Uhlmann. An immersed boundary method with direct forcing for the simulation of particulate flows. *Journal of Computational Physics*, vol. 209 (2005), no. 2, pp. 448–476.

[14] D. Weaire, N. Pittet, S. Hutzler, and D. Pardal. Steady-state drainage of an aqueous foam. *Physical Review Letters*, vol. 71 (1993), no. 16, pp. 2670–2673.

[15] A.T. Dinsdale and P.N. Quested. The viscosity of aluminium and its alloys – a review of data and models. *Journal of Materials Science*, vol. 39 (2004), no. 24, pp. 7221–7228.

[16] A. Hazen. Experiments upon the purification of sewage and water at the lawtence experiment station. *Massachusetts States Board of Health Twenty-Third Annual Report*, (1892), pp. 428–434.

[17] B. Hölting and W.G. Coldewey. *Hydrogeologie: Einführung in die Allgemeine und Angewandte Hydrogeologie* (Spektrum Akademischer Verlag, 2005).

[18] S. Heitkam, W. Drenckhan, and J. Fröhlich. Packing spheres tightly: influence of mechanical stability on close-packed sphere structures. *Physical Review Letters*, (2011), vol. 108 (20‘12), no. 14, p. 148302.

Received 16.02.2012